

**Fire performance of wood–steel hybrid elements  
finite element analysis and experimental validation**

Abdelrahman, Mostafa; Khaloian-Sarnaghi, Ani; van de Kuilen, Jan Willem

**DOI**

[10.1007/s00226-024-01628-0](https://doi.org/10.1007/s00226-024-01628-0)

**Publication date**

2025

**Document Version**

Final published version

**Published in**

Wood Science and Technology

**Citation (APA)**

Abdelrahman, M., Khaloian-Sarnaghi, A., & van de Kuilen, J. W. (2025). Fire performance of wood–steel hybrid elements: finite element analysis and experimental validation. *Wood Science and Technology*, 59(1), Article 23. <https://doi.org/10.1007/s00226-024-01628-0>

**Important note**

To cite this publication, please use the final published version (if applicable).  
Please check the document version above.

**Copyright**

Other than for strictly personal use, it is not permitted to download, forward or distribute the text or part of it, without the consent of the author(s) and/or copyright holder(s), unless the work is under an open content license such as Creative Commons.

**Takedown policy**

Please contact us and provide details if you believe this document breaches copyrights.  
We will remove access to the work immediately and investigate your claim.



# Fire performance of wood–steel hybrid elements: finite element analysis and experimental validation

Mostafa Abdelrahman<sup>1,2</sup> · Ani Khaloian-Sarnaghi<sup>1</sup> · Jan-Willem van de Kuilen<sup>1,3</sup>

Received: 13 August 2024 / Accepted: 16 December 2024 / Published online: 11 January 2025  
© The Author(s) 2025

## Abstract

Wood-steel hybrid (WSH) elements are gaining popularity in the construction industry due to their reduced environmental impact and high load capacity. However, fire resistance remains a crucial challenge for advancing wood as a construction material. The proposed WSH slab consists of a trapezoidal steel profile sandwiched between two laminated veneer lumber (LVL) beech panels. This research aims to numerically predict the fire performance of the proposed WSH slab element by generating heat transfer models that consider convection, radiation, and conduction. The objectives are to predict the temperature profile of the system's components, assess the charring rate of the LVL panels, and validate the results with experimental fire tests. Computed Tomography (CT) scanning was additionally used to detect the material density variation in the remaining LVL layers after fire tests. Simulations reveal that the size and shape of the internal cavity significantly influence heat flow within the system. Analysis of different thicknesses and heights of the steel sheet shows a substantial impact on the charring initiation time of the upper LVL layer. Temperature profiles of the components from numerical analysis exhibit similar behavior to that observed in the experiments. The experimental charring rate averages between 0.88–1.00 mm/min, while the numerical rate averages between 0.95–1.06 mm/min, with a 5–8% average deviation attributed to conduction interaction between LVL and the steel sheet. This variation may also be caused by the definition of generic thermal properties of wood according to EN1995-1-2, which may not accurately represent the behavior of the LVL element under fire.

---

✉ Mostafa Abdelrahman  
mostafa.abdelrahman@tum.de

<sup>1</sup> TUM School of Engineering and Design, Department of Materials Engineering, Technical University of Munich, Winzererstrasse 45, 80797 Munich, Germany

<sup>2</sup> Faculty of Engineering, Department of Civil Engineering, Suez Canal University, El Sheikh Zayed, 8366004 Ismailia, Egypt

<sup>3</sup> Faculty of Civil Engineering and Geosciences, Biobased Structures and Materials, Delft University of Technology, Stevinweg 1, Delft 2628 CN, The Netherlands

## Introduction

Wood and steel are widely common materials in modern construction due to their robustness, durability, and adaptability. Recently, there has been an increasing trend toward combining wood and steel into a single structural component. This hybrid approach leverages the strengths of both materials to enhance mechanical properties such as stiffness, durability, and strain capacity while mitigating disadvantages like high weight and high costs associated with traditional steel–concrete composites. Additionally, wood–steel hybrid elements contribute to sustainability by reducing the carbon footprint and speeding up construction processes through pre-fabrication (Ilgin et al. 2022; Balasbaneh et al. 2022). Wood–steel composites, also known as Wood–steel hybrid elements, are pre-lab clean, fast, and dry lightweight solutions that can cover long spans without adhesives, using mechanical fasteners between wood and steel elements, while also allowing cavities for insulation and different building utilities. The combination of wood in form of a composite with steel offers several benefits, such as low energy consumption, low carbon emissions, and a high strength-to-weight ratio. Steel provides high strength and homogeneous properties. However, for thin, cold-formed steel members, achieving maximum strength can be challenging due to local buckling and deformation (Tsai and Koshihara 2014; Yadav et al. 2022). Wood–Steel Hybrid Elements have many applications in the construction market, such as beam sections, structural slab systems, frames, and truss systems.

However, fire resistance remains a critical challenge for wood–steel hybrid elements. At high temperatures, the various chemical components of wood undergo thermal degradation, and the degradation level is dependent on the temperature and duration of exposure. At temperatures below 100 °C, due to the depolymerization process, wood suffers a continuous decrease in tensile strength. Between 100 and 200 °C, water evaporates, hydrating wood and producing noncombustible gases such as acetic acid, formic acid, and CO<sub>2</sub>. Around 200 °C, dehydration reactions dominate the pyrolysis of lignin, producing a large amount of char for wood. From 200 to 300 °C, the wood starts to produce high amounts of carbon monoxide, and the hemicellulose and lignin components are pyrolyzed. Around 300 °C, aliphatic side chains break off from the lignin's aromatic ring, and the wood cellulose depolymerizes at temperatures between 300 and 350 °C. The carbon–carbon bond between lignin structural units breaks down at temperatures between 370 and 450 °C. At higher temperatures, the residual wood becomes an activated char called “afterglow.” (White and Diertenberger 2010). Wood density is reduced as a result of thermal degradation. Fonseca et al. (2012) and Tabaddor et al. (2008) reported in their research that the charring front temperature of wooden elements begins in the temperature range of 280–300 °C. Although the charred layer reduces the cross-sectional area of the element and weakens its structural integrity, it is still very important in protecting the entire element during fire conditions compared to other building materials. In addition, it is possible to determine the rate at which the charring progresses through the element and assess the effectiveness of a suitable insulation system (Fonseca 2024). In

engineered wood products such as laminated veneer lumber (LVL), a charring layer develops after ignition, decreasing the material's strength and load-carrying capacity. The char layer protects the remaining wood, resulting in a consistent charring rate through the element (Harada et al. 2006; Fragiaco et al. 2013). Crielaard et al. (2019) reported that using wood products such as cross-laminated timber (CLT) may not be efficient in directly fire-exposed situations. This is because CLT may delaminate under such conditions, and the delaminated material contributes to the fire by increasing heat release and extending its duration.

On the other hand, Steel sections, particularly cold-formed steel (CFS) members, undergo different mechanical and thermal behavior under high temperatures. Steel's high thermal conductivity and surface-to-volume ratio make it more susceptible to fire damage. Unprotected, fire-exposed steel sections exhibit a rapid increase in temperature, leading to a significant loss in strength and stiffness. The thermal degradation of CFS influences the section's mechanical properties, such as yield strength and modulus of elasticity, as well as alterations in their thermal properties, such as thermal conductivity, thermal elongation, and specific heat (Abreu et al. 2014; Hsu et al. 2016; Hassanieh et al. 2016).

The fire performance of Wood-Steel Hybrid (WSH) elements was investigated in most of the research on components such as beam elements and wood-steel bolted connections. Nguyen et al. (2023) demonstrated in their study that wood is highly effective as a passive fire protection material for steel in hybrid systems. In such cases, wood significantly delays the time to reach the critical temperature of 550°C (35–40 min compared to 5–10 min for unprotected steel, which can even reach temperatures as high as 1200°C). Petrycki et al. (2019) conducted an experimental study on wood-steel connections under fire exposure, investigating the behavior of Glued-laminated timber (glulam) bolted connections in fire conditions. Their study revealed that the time to failure of the loaded connections is primarily governed by the shear resistance of the wooden elements. Le et al. (2019a, 2019b) studied the fire resistance of 12 WSH structural beams in fire tests with a duration of 60 min. The findings showed that the temperatures at the steel flanges increased by over 300 °C in 10 out of 12 WSH beams during the last 5 min of the experiment. In addition, structural degradation was assessed. The study suggested increasing wood thickness to enhance fire resistance.

Regarding the cavity influence in the fire resistance of the elements, Fonseca et al. (2013) investigated the fire performance and thermal analysis of wooden cellular slabs experimentally and numerically on two timber slabs with rectangular holes under different fire exposure times of 1500 s and 900 s. The analysis of the charred layer confirmed that wooden slabs containing internal cavities exert a substantial influence on the charring rate. This influence is contingent upon both the shape and size of the cavity. Furthermore, Frangi et al. (2008) studied the influence of a lower protection layer on the charring rate in timber frame floor assemblies with void cavities. The results of that study revealed that after the failure of the fire-protective claddings, both elevated fire temperatures as well as the heat energy that is emitted through radiation within the cavity play substantial roles in the accelerated charring rate of suddenly exposed timber slab components.

Various techniques have been developed for assessing the charring rate of wooden elements by measuring the depth of the charred layer after the fire test as described in Frangi et al. (2003, 2008) and Fahrni et al. (2018a, 2018b, 2021). The recent approach used by Fahrni et al. (2021) involves the analysis and visualization of this data as a colorized 3D model generated using Autodesk Recap Photo 20.0.1.5. This method includes scanning the specimen after removing the char layer using optical techniques, capturing images from diverse viewpoints and angles with consistent camera settings and focal length. Just et al. (2010) used the ATOS (Advanced Topometric Sensor) II scanner to analyze the charred cross-section of wooden wall studs subjected to fire conditions. Reference targets were used in this study to establish a consistent coordinate system and ensure the visibility of the targets during scanning. The collected data were exported to computer-aided design software for establishing three-dimensional models.

The experimental studies proved to be cost-intensive, complex, and required stringent safety protocols. Therefore, having a validated numerical model may help to simulate and predict the thermal behavior of the components under fire. Key parameters to consider in studying the fire behavior of wooden elements include the temperature development within the section under fire (time–temperature profile) and the charring rate of the wooden element. When developing numerical models to simulate the fire performance of timber elements, it is essential to include all three modes of heat transfer: convection, radiation, and conduction, in order to simulate the real-case fire behavior and to predict the thermal response of the material. These mechanisms significantly influence temperature distribution, charring rates, and overall structural response during fire. Neglecting any of these modes can lead to inaccuracies in predicting the behavior of timber elements under fire conditions (Incropera et al. 2013). The study by Thi et al. (2016) presented a numerical model for heat transfer in timber structures exposed to fire, integrating conduction, radiation, and convection based on the Fourier heat equation. The model parameters were calibrated using experimental data on laminated veneer lumber (LVL), achieving close agreement with measured temperatures from the experiments (within 4.74% at 40 min of exposure). The model also simulated the formation of the charring layer considering 300°C as char front temperature, validating the model against the actual behavior observed in experiments. Couto et al. (2016) and Fonseca et al. (2013) evaluated the behavior and performance of timber slabs with rectangular holes during fire exposure experimentally and numerically using the finite element method. Their evaluation of the charred layer confirmed that cavities influence the charring rate of the upper side of the element. Špilák et al (2022) provided a numerical model based on the enthalpy approach to determine the charring layer of wooden elements, addressing issues associated with incorrect results at temperatures around 100°C. Their numerical temperature profiles achieved 91.7% accuracy, and the simulation of the charring layer area was 93.0% accurate compared to experimental tests. Other researchers, such as Zhang et al. (2012) and Molina et al. (2012), developed numerical models to simulate fire and heat transfer for timber beams and validated these models with experimental tests. Deviations were observed between the numerical and experimental temperature profiles in those studies. Concluding

that such deviation might occur due to an increased amount of heat, entering the pyrolysis zone during the test, thereby increasing the temperature with unpredictable behavior.

This paper focuses on analyzing the fire performance of wood-steel hybrid (WSH) slab elements made of trapezoidal cold-formed steel profile sandwiched between two layers of laminated veneer lumber (LVL) panels. Using both experimental and numerical methods, the study investigates how cavity size and steel profile thickness influence the behavior of the wooden element under fire conditions. The research aims to predict the overall fire performance of the system by validating the numerical temperature profiles of the materials and the charring rate of the LVL panels. Additionally, the study assesses the charring rate of the LVL layers and uses computed tomography (CT) scanning to analyze density variations in the wood after fire exposure.

## Material and methods

### Laboratory experiments

Four experiments were performed on wood steel hybrid element (WSH). Each specimen consisted of three main components, as illustrated in Fig. 1 and Table 1:

- Two laminated veneer lumber (LVL) panels made of beech wood ( $a \times b \times t_p$ )  $500 \times 500 \times 36 \text{ mm}^3$  provided by Pollmeier (Pollmeier 2017).
- Corrugated steel plate with two different geometries M ( $h \times b$ )/ $t_s$ , where  $h$  represents the height of the steel profile,  $b$  represents the width between the flanges, and  $t_s$  represents the thickness of the steel profile (Münker 2020).
- Connection between the wood and the steel components, which is typically provided by mechanical fasteners using metal screws.

### Material properties and temperature measurement

LVL "Beech Wood-BauBuche" from Pollmeier was used in this study, with mechanical properties sourced from the provider's datasheet (Pollmeier 2017). The mean

**Fig. 1** Wood-Steel Hybrid slab components

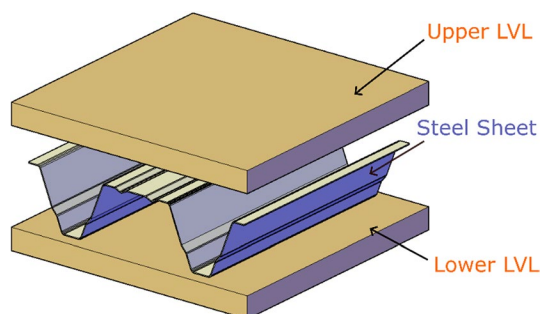


**Table 1** WSH specimens components and dimensions prepared for fire test

	S1	S2	S3	S4
Upper LVL panel ( $a \times b \times t_p$ )	500 × 500 × 36 mm			
Steel Sheet ( $M(h \times b)/t_s$ )	$M(100 \times 275)/0.75$ mm	$M(100 \times 275)/1.25$ mm	$M(150 \times 280)/0.75$ mm	$M(150 \times 280)/1.25$ mm
Lower LVL panel ( $a \times b \times t_p$ )	500 × 500 × 36 mm			

density was  $800 \text{ kg/m}^3$ , and the characteristic density was  $730 \text{ kg/m}^3$ . The bending strength was  $75 \text{ N/mm}^2$ , and the mean modulus of elasticity was  $16,800 \text{ N/mm}^2$ . For the corrugated steel profile, according to the provider's datasheet (Münker 2020), the characteristic density of the steel plates was  $7,890 \text{ kg/m}^3$ , with a modulus of elasticity of  $200 \text{ GPa}$  and thermal conductivity ( $\lambda$ ) of  $0.038 \text{ W/mK}$ . For the mechanical fasteners between the trapezoidal steel plate and both upper and lower LVL panels, Self-drilling timber-metal screws (SBS) with dimensions  $\text{M4.2} \times 30 \text{ mm}$ , supplied by Rothoblaas (2010), were used. The screws had galvanized surfaces with mechanical properties according to DIN EN 14592:2012.

To perform accurate temperature measurements in fire tests, the temperature measurement device should fulfill two crucial criteria: (a) accurately display temperatures within the specimen and (b) refrain from disrupting its temperature distribution. Two types of thermocouples were used in this study for registration of the temperature. The first type was the wire thermocouple (type K) (TCs-1), known as Chromel–Alumel thermocouple, which was used to record the temperature in three positions at the middle of LVL panels during the experiment. The second type of thermocouple was the one with copper disc (TCs-2), which was used to record the temperature at the inner surfaces of the LVL panels and steel profile. To ensure the accuracy of the measurements, all the thermocouples were tested, using a digital thermometer prior to installation.

Thermocouples (TCs-1) were installed at the depth of  $18 \text{ mm}$  in the middle of both upper and lower LVL panels, and were set at three different positions: One at the center of the board and the others shifted  $150 \text{ mm}$  up and down to the middle position. Thermocouples with copper discs (TCs-2) were installed in the middle of the inside surfaces of both upper and lower LVL panels, and in two positions:  $100 \text{ mm}$  up and down the center axis of the boards. In total three TCs- 1 and two TCs-2 have been installed per panel, as shown in Fig. 2a. In order to guarantee that the thermocouples with copper discs (TCs-2) stay fixed on its position on the inside surfaces of the boards during the test, each thermocouple was fixed with an inorganic insulating pad bonded with non-combustible fire resistance adhesive. The insulating pad material has a density within the range of  $900 \pm 100 \text{ kg/m}^3$ . For recording the temperature change of the trapezoidal section during the test, thermocouples with copper discs (TCs-2) were used at the middle of the section in three different positions: Lower stiffener, inclined surface, and upper stiffener. Thermocouples' discs were fixed to the surface of the metal sheet using the insulating pads over the copper discs of (TCs-2), similar to the method described previously, as shown in Fig. 2b. Thermocouples were numbered and arranged systematically to facilitate the monitoring and analysis of recorded temperatures during and after the fire test. A 3D drawing illustrating the positions of the thermocouples along with their respective numbers is provided in Fig. 3.

## Specimens assembly and experiment procedure

The specimens were prepared and stored in a climate-controlled room for three weeks before testing to achieve an equilibrium moisture content of  $12.5\%$ . After



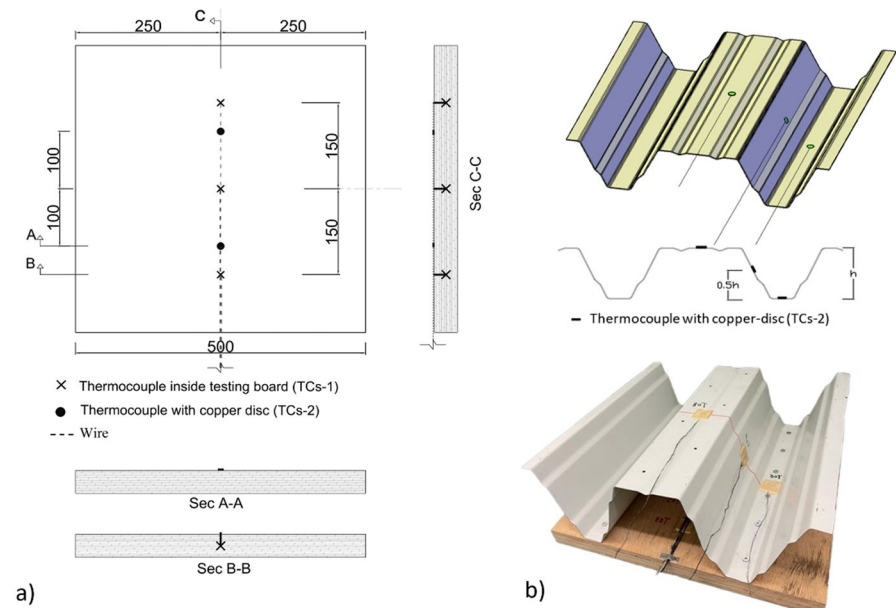


**Fig. 2** Thermocouples installation: **a** LVL panels, **b** trapezoidal steel profile

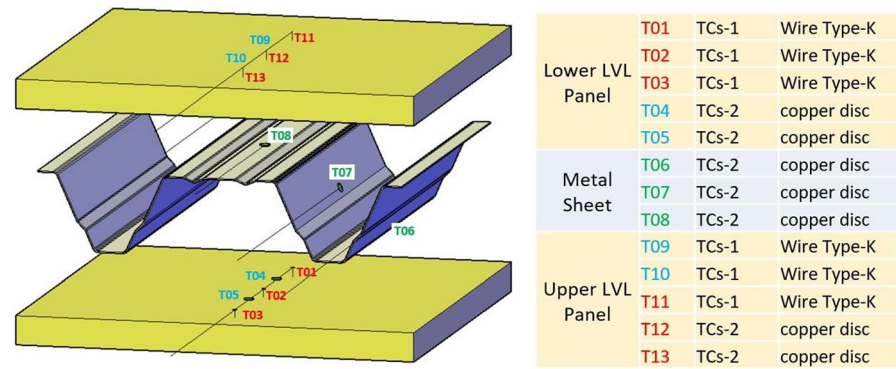


**Fig. 3** Thermocouples positions and numbers for temperature recording during the fire test

assembly, all four sides of each specimen were covered with a 15 mm calcium-sulfide insulation board, sealed with non-combustible fire-resistant adhesive to prevent additional oxygen ingress during testing and to ensure a controlled one-dimensional heat flow, as shown in Fig. 4. The insulation surrounding the specimen surfaces parallel to the heat flow direction should ideally create an adiabatic boundary. Insufficient insulation at these surfaces could allow cooling from ambient air or cause heat loss perpendicular to the intended charring direction, reducing charring near those areas (Fahrni et al. 2021). The experiments were conducted using a



**Fig. 4** WSH slab specimen: **a** WSH specimen after assembly, **b** WSH specimen after side insulation, **c** specimen mounting system

vertically fixed furnace equipped with a single oil burner, with temperature regulation managed by a thermometer placed approximately 150 mm behind the specimen. The furnace was maintained at a pressure of  $-5\text{Pa}$  relative to ambient pressure and controlled according to the time–temperature standard outlined in EN 1363–1 (2012). In order to achieve a one-dimensional charring, the furnace’s installation is required to guarantee a one-dimensional heat flow during the test. Fiberglass tapes were employed around the furnace frame to ensure consistent charring of the lower LVL panel and to block additional air from entering the ignition zone during the test. A supporting system was installed on the specimen to prevent any movement that could lead to stability issues during the test, as shown in Fig. 4c.

### CT-scan

Computed tomography scanning (CT-scan) was used to scan the four remaining upper LVL panels of the four specimens before removing the charring layer. After the fire test, the LVL panels were extinguished with water and left to air-dry naturally for two days to remove residual moisture from the sections. They were then stored in a climate-controlled chamber at 65% relative humidity and  $20^{\circ}\text{C}$  for three weeks to stabilize before scanning.

In addition to the four LVL panels, an uncharred LVL panel was scanned as a reference panel, in order to compare the veneers’ behavior before and after fire exposure (Fig. 5). Philips Ingenuity 128 multi-detector computed tomography scanner (Philips Healthcare, Best, Netherlands) with  $0.3 \times 0.3 \times 0.8 \text{ mm}^3$  spatial resolution using a high-resolution reconstruction kernel (YB), 120kVp and 200m was used for CT scanning of the samples. *MicroDicom 2.7.9* and *RadiAnt DICOM Viewer 4.2.1* were used as the visualization software for the CT-scan images. By segmentation of the CT-scan data, nine different positions were selected on the sample, where density variations have been studied along the defined paths over the thickness of the samples. *ImageJ* was used for analyzing the CT scan data. The measurements were conducted based on three sectional cuts: sec a, sec b, and sec c, which were made at 150 mm above the centerline, the centerline of the specimen, and 150 mm below the centerline, respectively. The charring rates (mm/min) for the upper LVL panels were determined by dividing the charring depths (mm) by the fire duration (min). To prevent any influence from corner rounding, 50 mm of the outer perimeter

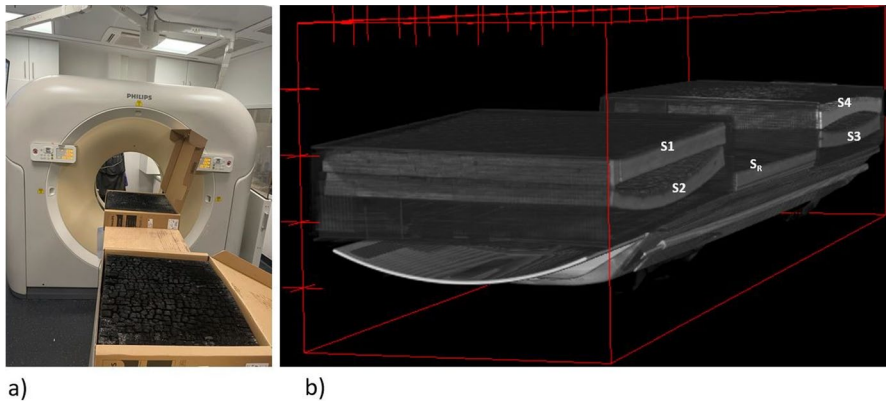


**Fig. 5** Applying CT-scan on upper LVL panels: **a** entering the specimens to the scanner, **b** specimen's layout with their numbers in the scanner

of each panel was excluded from the charring depth analysis. Only the inner area of  $400 \times 400$  mm was analyzed.

After scanning the panels, the charred layers on the LVL panels were removed, in order to determine the charring depth of the upper LVL panels. Manual cleaning was used to avoid applying any pressure on the specimen, which may happen when using an automatic angle grinder brush. According to Eurocode 5, the charring line is the layer of material formed between the charred layer and unburnt wood. This line forms at a temperature of  $300^{\circ}\text{C}$ . Therefore, the start of the fire duration for the upper LVL panel was determined when the thermocouples on the inner surface of the panel reached  $300^{\circ}\text{C}$ . Similarly, for the lower LVL panel, which was completely burnt, the start of the fire duration was determined when the temperature of the outer surface of the panel (exposure surface) reached  $300^{\circ}\text{C}$ , and the end of the fire duration was determined when the temperature of the inner surface of the panel reached  $300^{\circ}\text{C}$  (König 2005).

## Numerical simulation

The fire performance of the system was simulated through a heat transfer model developed in ABAQUS. This model was then validated with the experimental results by comparing the temperature profiles, as well as the charring rates from both methods. An unsteady-state heat transfer analysis, or transient analysis, is appropriate for studying the thermal properties of a certain material under fire exposure over time. The time period of the analysis represents the duration of the fire. Three modes of heat transfer were considered in the simulations: radiation, convection, and conduction. Radiation and convection occur at the furnace, where the burner emits heat towards the first LVL panel, heating the air in the testing zone and transferring heat to the surface of the specimen. Conduction is considered within the element's thickness and between the LVL panels and the steel sheet.

According to Fourier's law, the heat flux is proportional to the temperature gradient as shown in Eq. 1 (Incropera et al. 2013):

$$\rho C_p \frac{\partial T}{\partial t} = \frac{\partial}{\partial X} \left[ \lambda \frac{\partial T}{\partial X} \right] + \frac{\partial}{\partial y} \left[ \lambda \frac{\partial T}{\partial y} \right] + Q_r'' \quad (1)$$

where  $T$  [K] represents the temperature,  $x$  [m] and  $y$  [m] are the spatial coordinates, and  $t$  [s] is the time. The material properties are characterized by the parameters  $\lambda$  [W/(m·K)] for thermal conductivity,  $\rho$  [kg/m<sup>3</sup>] for density, and  $C_p$  [J/(kg·K)] for specific heat capacity, while  $Q_r$  [W/m<sup>3</sup>] denotes internal heat generation.

Initial temperature distribution throughout the domain was defined according to Eq. (2).

$$T_{(x,y,z,0)} = T_0 \quad (2)$$

Neumann Boundary Condition (Eqs. 3 and 4) specifies the heat flux normal to the boundary, which represents the convection and radiation behavior.

$$-\lambda \frac{\partial T}{\partial n} = q \quad (3)$$

$$-\lambda \frac{\partial T}{\partial n} = h_{conv} (T - T_\infty) + \sigma_{Boltz} * \epsilon * (T^4 - T_\infty^4) \quad (4)$$

where  $T_0$  is the initial temperature,  $q$  is the prescribed heat flux and  $n$  is the normal vector to the boundary. The convection coefficient  $h$  [W/(m<sup>2</sup>·K)] characterizes the rate of heat transfer via convection.  $T_\infty$  [K] denotes the temperature of the furnace environment. The Stefan-Boltzmann constant  $\sigma_{Boltz}$  [W/(m<sup>2</sup>·K<sup>4</sup>)] is  $5.67 \times 10^{-8}$ , representing the constant in the Stefan-Boltzmann law.  $\epsilon$  represents the emissivity coefficient, which describes the material's ability to emit radiation relative to a perfect blackbody.

The temperature-dependent material properties for both LVL panels and the steel sheet were defined according to (EN 1993-1-2 2004; EN1995-1-2 2004), respectively (Fig. 6). The density of the steel was considered temperature-independent with a value of 7850 kg/m<sup>3</sup> according to the supplier's datasheet. Thermal conductivity was considered to be isotropic. Isotropic properties provide sufficient accuracy for modelling of the overall heat transfer and charring behavior of the wood-steel hybrid system in this study. The density of the LVL panel was defined as temperature-dependent due to the mass loss of the material during the fire. The initial density of LVL was taken as 730 kg/m<sup>3</sup> based on the supplier's datasheet (Pollmeier 2017). Temperature dependent density variation of timber has been defined based on the graphs in (EN1995-1-2 2004). For unforced natural air surrounding a flat surface the convection coefficient is considered to be 25 W/(m<sup>2</sup>·K), while The emissivity coefficient  $\epsilon$  is considered (0.8) for wood and (0.3) for the steel. C3D8 elements was used for the FE-analysis.

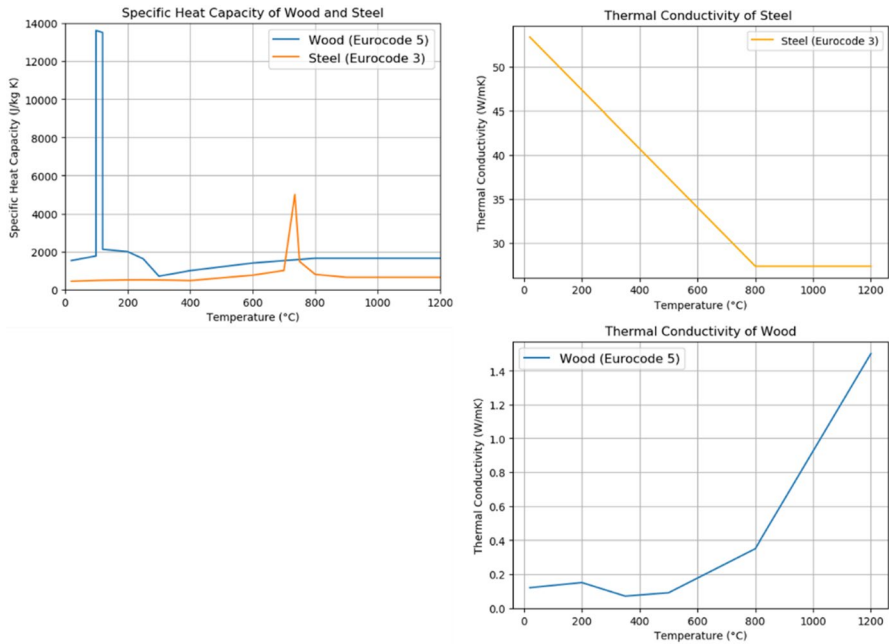


**Fig. 6** Thermal properties of wood and steel with temperature dependency (EN 1993-1-2, 2004; EN1995-1-2, 2004)

**Interaction and boundary conditions**

Tied constraint was used to ensure the contact behavior between the steel plate and the LVL panels within the simulations. This constraint ensures that each node on the slave surface matches the temperature of the corresponding point on the master surface, thereby maintaining uniform thermal conditions across the contact interface, as shown in Fig. 7. The initial system temperature was set to ambient room temperature (25°C).

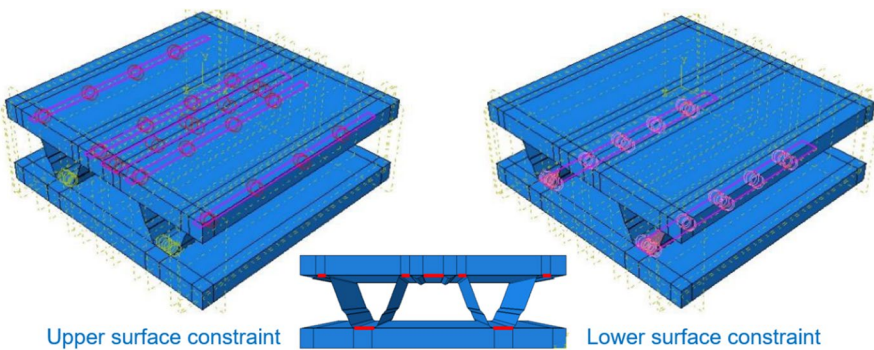


**Fig. 7** Interactions between the steel sheet and the LVL surfaces for both upper and lower panel

The heat flux, calculated from Eq. 4 and representing convection and radiation from the heating source (furnace burner), was applied in two stages:

**1. First stage:** From the start of the test until the lower LVL panel was burned (50~55 min), a surface heat flux was applied on an area of  $450 \times 450$  mm on the lower LVL panel surface, representing the furnace opening using ( $T_{\infty}$ ), the temperature of the furnace from the experiment (Fig. 6).

**2. Second stage:** After the lower LVL panel was burnt, the surface of steel sheet was directly exposed to the furnace burner until the end of the experiment (80 min for S1 and S2, 90 min for S3 and S4), when the. A heat flux was applied

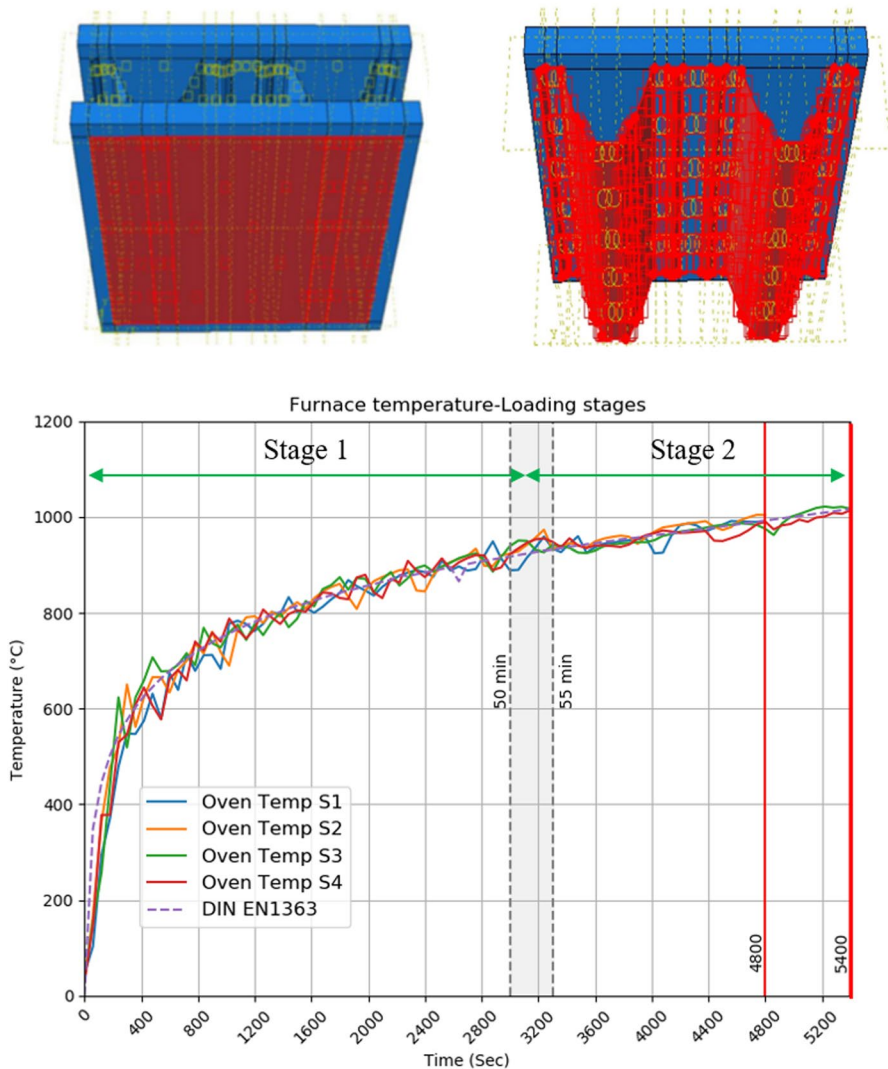


**Fig. 8** Furnace's temperature amplitude with areas of applying heat flux (first and second stage)



to the steel sheet surface using ( $T_{\infty}$ ), the temperature of the furnace for this time period (Fig. 8).

The start time and exposure rate of the steel sheet to the furnace burner were determined based on the results from stage one of the simulation. As shown in Fig. 8, it took approximately 50 to 55 min for the entire upper surface of the lower LVL panel to reach the 300°C threshold.

## Results and discussion

### Experimental results

#### Temperature profiles and visual observations

During the fire tests, small cracks started to appear on the lower LVL panel of all specimens, and the crack widths increased gradually with rising temperature and prolonged exposure time. In Fig. 9, the average temperatures at each position measured on sample S1 by the thermocouples are plotted over time, illustrating the behavior of the lower LVL panel at each time interval. Figure 10 presents time–temperature mean profiles of samples S2, S3, and S4. It shows that the lower LVL panels in all specimens were completely burnt. The remaining components, including

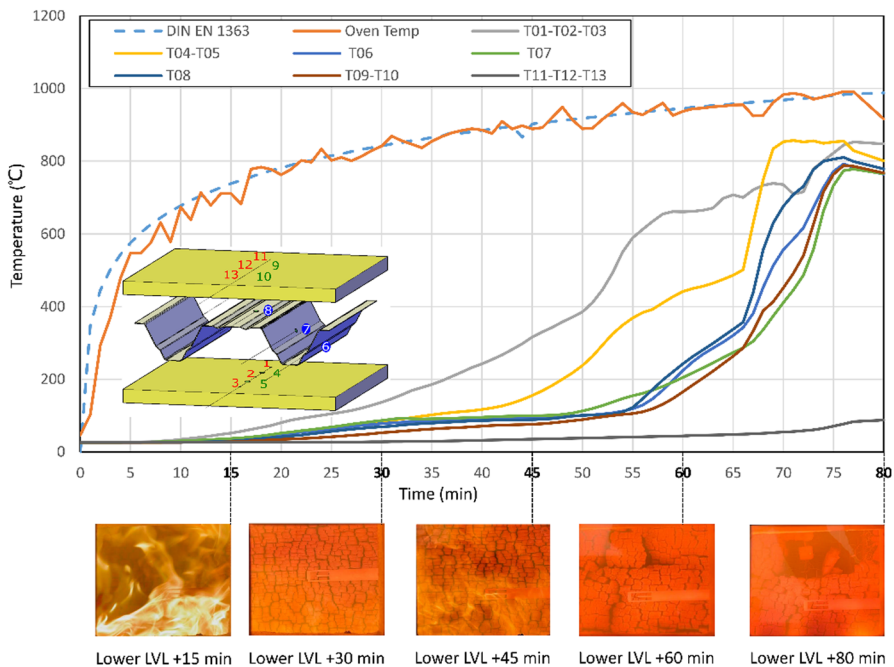


**Fig. 9** Time–Temperature Mean profile, specimen S1, showing the influence of the fire on the lower LVL panel after 15 min, 30 min, 45 min, 60 min, and 80 min

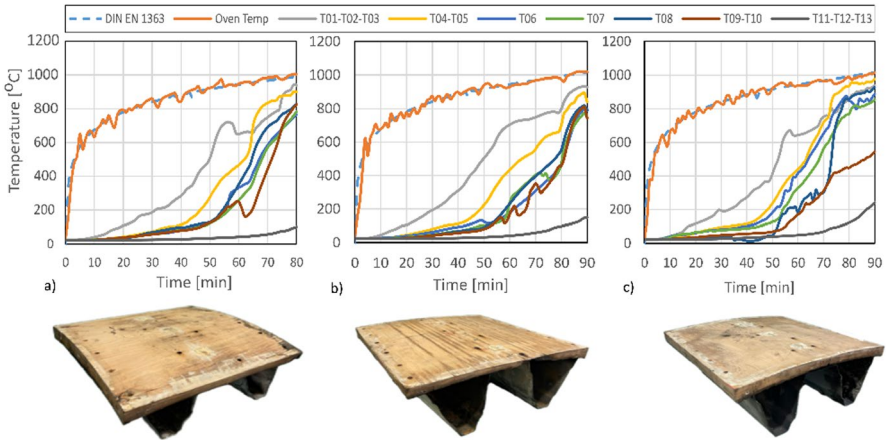


**Fig. 10** Time- Temperature profiles of specimens S2, S3, and S4

the steel plates and the upper LVL panels, were thermally degraded by fire. Temperature profiles recorded by surface thermocouples T09 and T10 in specimens S2 and S3, fixed to the inner surface of the upper LVL, exhibited oscillations. These oscillations occurred especially between temperatures of 200°C and 350°C when the upper LVL surface began to ignite, and a charring layer started to form beneath the thermocouples.

### Charring behavior

The upper LVL panels were scanned using a CT scanner, and the charring depth of each sample was determined through three sectional cuts. Three cuts were analyzed: A, B, and C. Cut B corresponds to the centerline of the layer, while cuts A and C are located 150 mm to the left and right of the centerline, respectively. These results are presented alongside the actual sections with the charred layer. The arrangement is illustrated in Fig. 11. The maximum charring depths for specimens S1, S2, S3, and S4 were 18 mm, 20 mm, 19 mm, and 22 mm, respectively recorded at the middle of the panel, where it was connected to the steel profile, highlighting the influence of heat conduction in this region. The charring line—the line between the burnt and unburnt wood—is clearly visible in the pictures of the CT-scanned LVL panels before removing the charring layer.

The average charring rate (mm/min) of the upper and lower LVL panels for specimen S1 is analyzed in Fig. 12, indicating the starting and ending points of the fire exposure for each panel, which is set to a char front temperature of 300°C. Table 2 presents the charring rate of the upper LVL panel for each specimen at different sectional cuts, along with the average charring rate of the lower LVL for each specimen. The charring rate for the lower LVL panel averaged between 0.7 and 0.73 mm/min, aligning closely with the recommended charring rate of 0.7 mm/min as per Eurocode 5 (EN1995-1-2 2004).



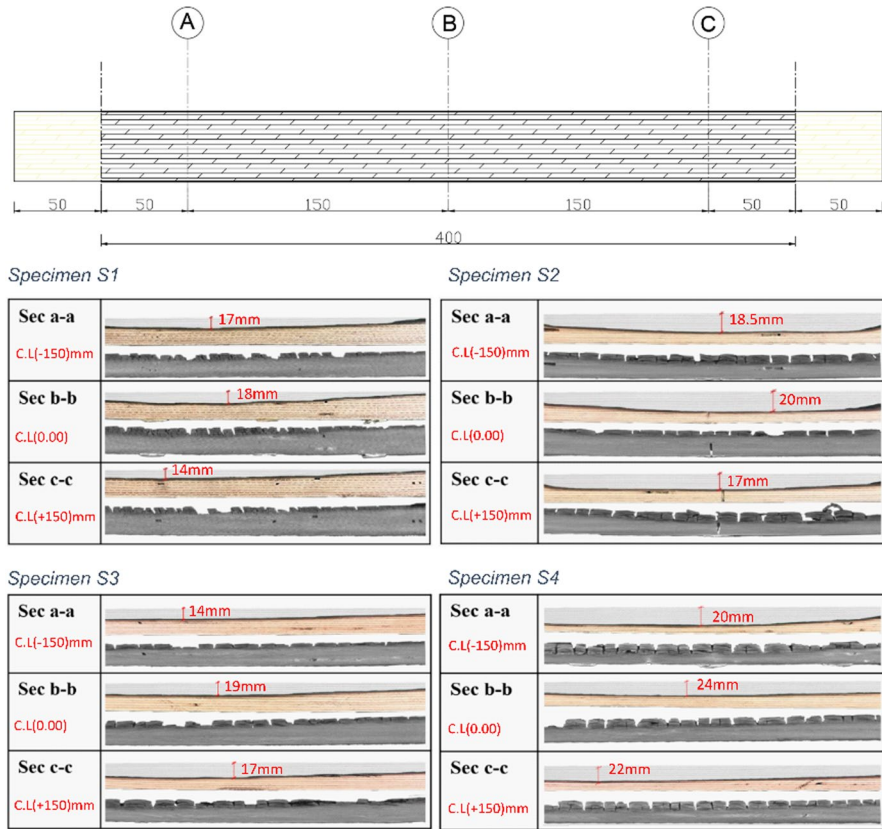


**Fig. 11** Charring depths of the upper LVL panels after removing the charring layer in three different sections A, B, and C. with corresponding CT scan sections

The charring rate of beech LVL panels, with an average density of  $777 \text{ kg/m}^3$  at 12% moisture content is found to range between 0.68 and 0.72 mm/min (Ehrlenspiel and van de Kuilen 2012). This is also corresponds to the findings of Moss et al. (2009) on LVL made from radiata pine, where charring rates fell within the range of 0.65 to 0.71 mm/min. Additionally, studies on the fire resistance of radiata pine LVL, with an average density of  $610 \text{ kg/m}^3$  at 13% moisture content (O'Neill et al. 2013), reported an average charring rate of 0.72 mm/min, further supporting the consistency of results. Fire experiments on radiata pine LVL, with an average density of  $605 \text{ kg/m}^3$  at 12% moisture content (Fragiacomo et al. 2013), revealed charring rates ranging from 0.69 to 0.83 mm/min on LVL panels. Based on this comparison, the density represents an effective factor in the charring rate of LVL elements. Moreover, the thickness of the steel sheet proved to be a critical factor affecting charring depth and rate in this study. Specimens S2 and S4, connected to an upper LVL panel with a 1.25 mm thick steel sheet, demonstrated more significant thermal deterioration compared to specimens S1 and S3, which were connected to

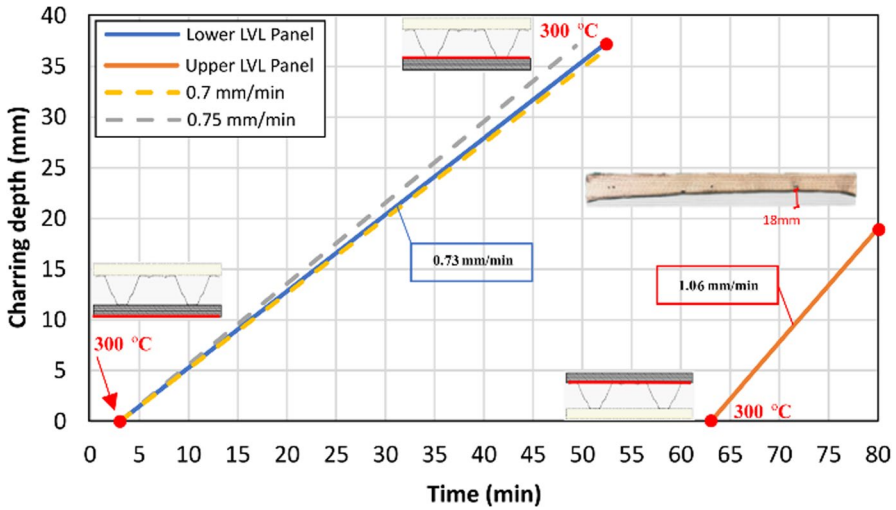


**Fig. 12** Average charring rate for upper and lower LVL panels of sample S1

**Table 2** Average charring rate (mm/min) for upper and lower LVL panels

Specimen		S1	S2	S3	S4
Lower LVL		0.73	0.73	0.70	0.73
Upper LVL	Sec(a-a)	1.00	0.92	0.76	1.04
	Sec(b-b)	1.06	0.95	0.88	1.00
	Sec(c-c)	0.95	0.90	0.81	0.98

a 0.75 mm thick steel sheet (Fig. 13). This outcome contradicts initial expectations, revealing that thicker steel sheets led to higher heat energy transfer to the upper LVL layer, thereby influencing its charring behavior. One potential explanation lies in the concept of thermal mass, where thicker materials have a greater capacity to absorb and store heat energy. Yanchun et al. (2021), in their heat transfer experiments involving steel plates of varying thicknesses, observed that thicker steel plates exhibit higher thermal mass, enabling them to store more heat and cool down more slowly compared to thinner steel plates. Thicker materials retain heat for extended periods, requiring more time to dissipate it effectively than thinner materials.

**Analyzing CT-scan and density variation**

By means of CT analysis (Freyburger et al. 2009; Lindgren 1992), the depth of charring in LVL and the uniformity of the density distribution were analyzed, as shown in the graphs in Figs. 14 and 15. Three sectional cuts (labeled V1, V2, and V3) were defined for each sample, and density variation was analyzed along these paths across the panel thickness. This procedure was conducted for nine different positions across each sample, revealing the density variations at the center

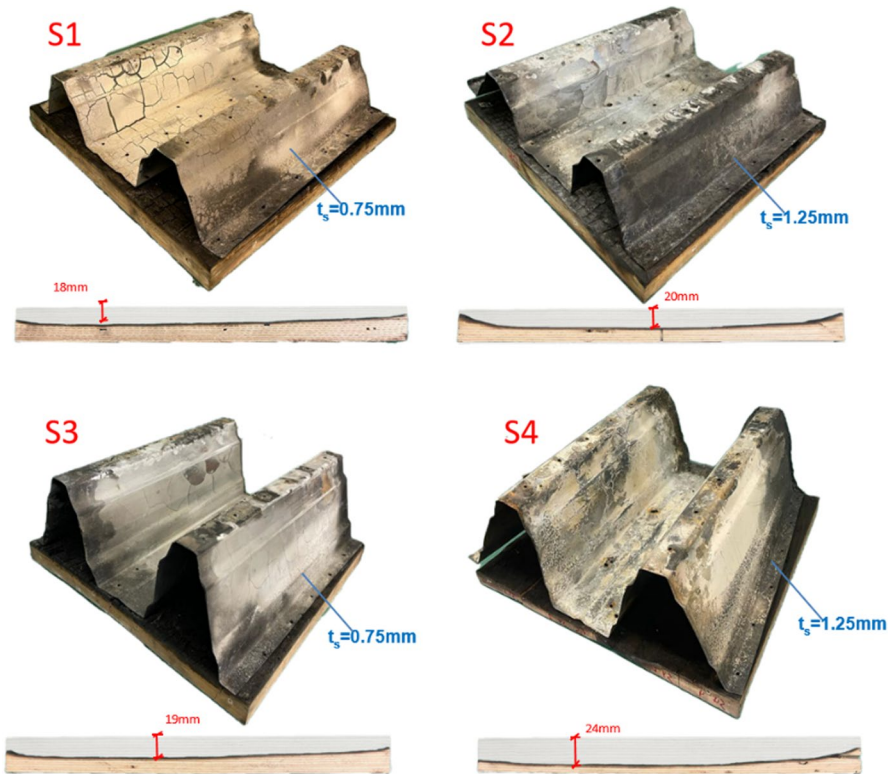


**Fig. 13** Maximum charring depth of the upper LVL panel for samples S1:S4, showing the influence of the steel thickness  $t_s$

and corners of the LVL panels. For comparative purposes, a reference sample (depicted in green) was included in each graph, showing a consistent density variation along the thickness without thermal exposure.

The results in Fig. 14 indicate that the solid parts of LVL panels, which did not experience high enough temperatures to burn, retained a density range similar to that of the reference sample. However, moving through the panel thickness, the density decreased due to moisture evaporation under elevated temperatures. While this observation aligns with expectations, the high scatter in material properties suggests that repeating the experiments under varying temperature conditions would help verify these results.

The charring depth at each position and for each sample was calculated by considering the total thickness of the LVL samples (36 mm) and identifying the point on each graph, where the density began to decrease, marking the boundary of burnt wood. These findings are summarized in Table 3 and Fig. 14. It can be seen in Table 3 that for most of the cuts, one side of the sample has higher charring depth compared to the other, related to the positioning of the sample at the CT-scanner. This can be validated from the pictures in Fig. 15. It can be seen in

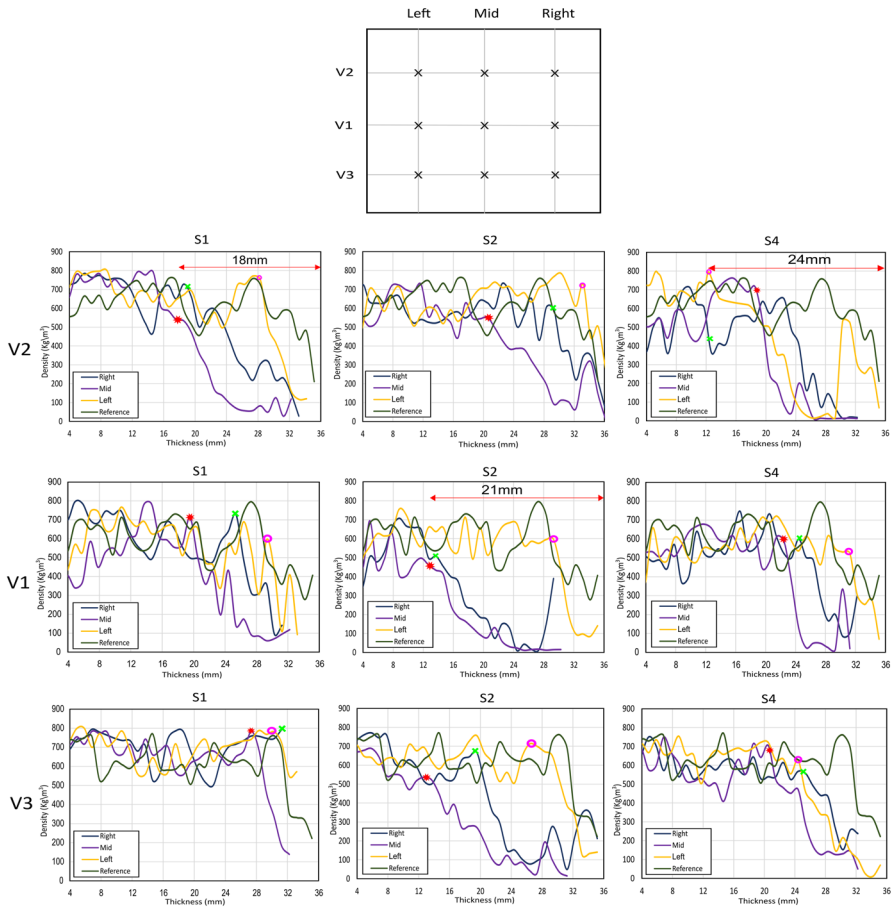


**Fig. 14** Density variation through the thickness of samples S1, S2, and S4

these figures that the material density distribution is not uniform over the surfaces. This may be due to the buckling of the steel plate under the high temperatures. Similar behavior can also be seen, when comparing the V-cuts. Samples S2 and S4 are the ones, which had steel plates with a thickness of 1.25 mm. This means that the heat transfer from the steel plate to those LVL samples that has been scanned (S2 and S4) have been higher. Therefore, bigger areas of fire failure can be observed in the CT images of those samples. Sample 4 was produced with a higher steel plate ( $h = 150$  mm). Therefore, one possible reason for the highly non-uniform burnt structure of the upper LVL in this sample may be the buckling of the steel plate and concentration of the heat transfer to a specific corner of the sample, as discussed before. In contrast, samples S1 and S2 with shorter steel plate ( $h = 100$ ) had a more uniform pattern of heat transfer. This can be visualized in Fig. 15, especially in the cut of the upper layer of these samples.

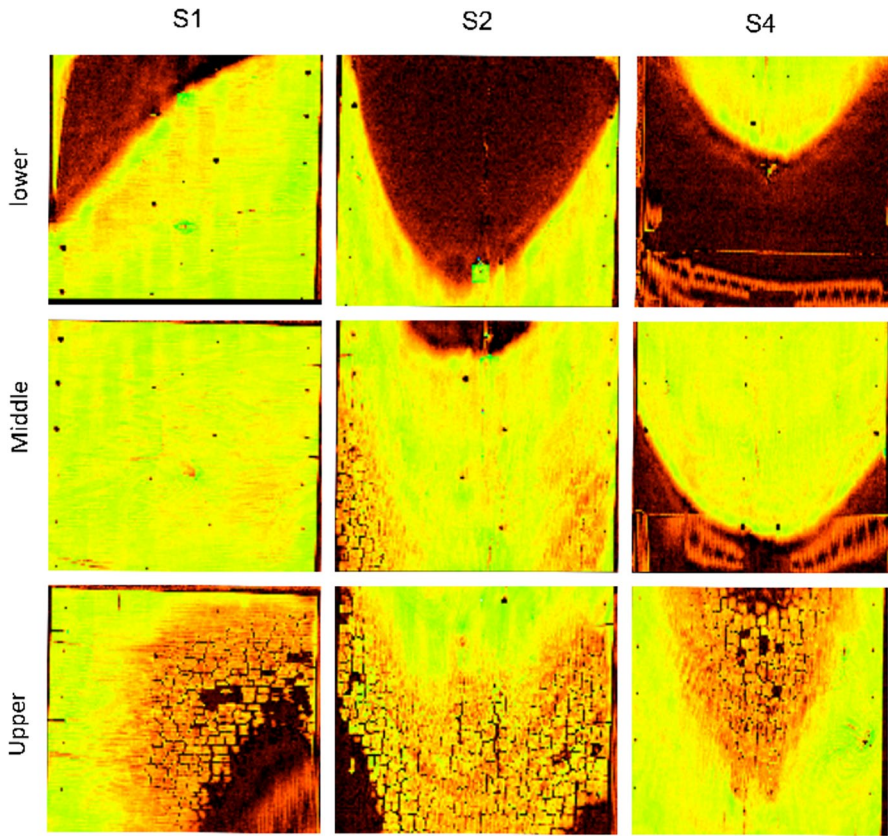


**Fig. 15** CT-scan images of the samples S1, S2 and S4

**Table 3** Charring depths (mm) calculated from the CT-scan images of the upper panels

		V2	V1	V3
S1	Right	14.54	11.61	5.75
	Mid	18.45	17.47	10.66
	Left	7.91	7.71	6.73
S2	Right	7.71	21.35	17.47
	Mid	15.52	23.35	22.38
	Left	3.79	7.71	8.71
S4	Right	14.12	11.64	11.64
	Mid	17.45	15.54	13.59
	Left	23.81	6.75	11.61



## Numerical validation

The numerical heat transfer models for different configurations of WSH systems (S1, S2, S3, and S4) are validated experimentally in terms of temperature profiles and charring behavior for the single components.

### Temperature profile of the component

Figure 16 shows the numerical temperature distribution for different configurations of WSH elements. It is notable that the contacted areas of the upper LVL panel to the steel profile experience higher temperatures than the uncontacted region. It is also observed that the samples with thicker steel sections transfer more heat than those with thinner sections (as represented by the difference between S2 and S1 for the 100 mm steel section height, and between S4 and S3 for the 150 mm steel section height).

### Lower and upper LVL panel

The numerical temperature profiles of the lower LVL panels show a slight deviation from the experimental temperature profiles, as shown in Fig. 17. This deviation starts at 2400 s and continues until 3000 s. During this period, heat begins to penetrate the lower LVL panel in the experiments through the screws connecting the steel sheet and the cracks formed in the charring layer, which are not presented in the numerical model. This phenomenon is also observed in the research of Zhang et al. (2012), who confirmed that the reason behind the deviations in numerical simulations from experimental results might be the formation of cracks through the charred layer at higher temperatures, which differs among different samples. Localized cracks in the charred layer increase the amount of heat entering the pyrolysis zone, thereby increasing the temperature unpredictably. After around 3000 s, both

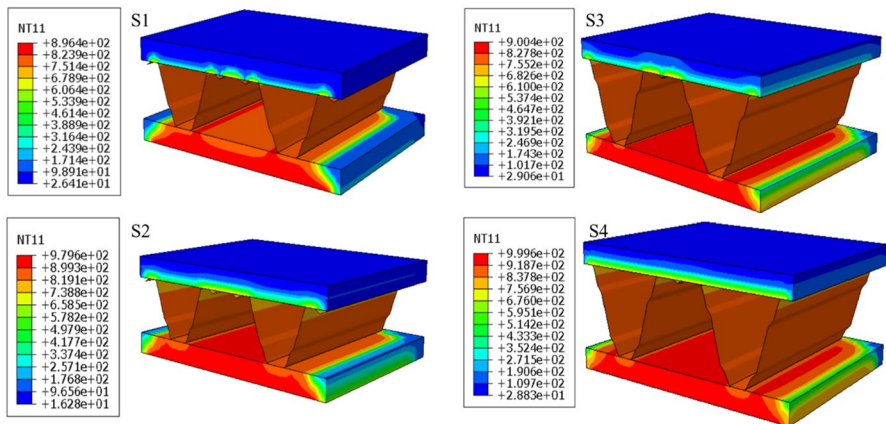
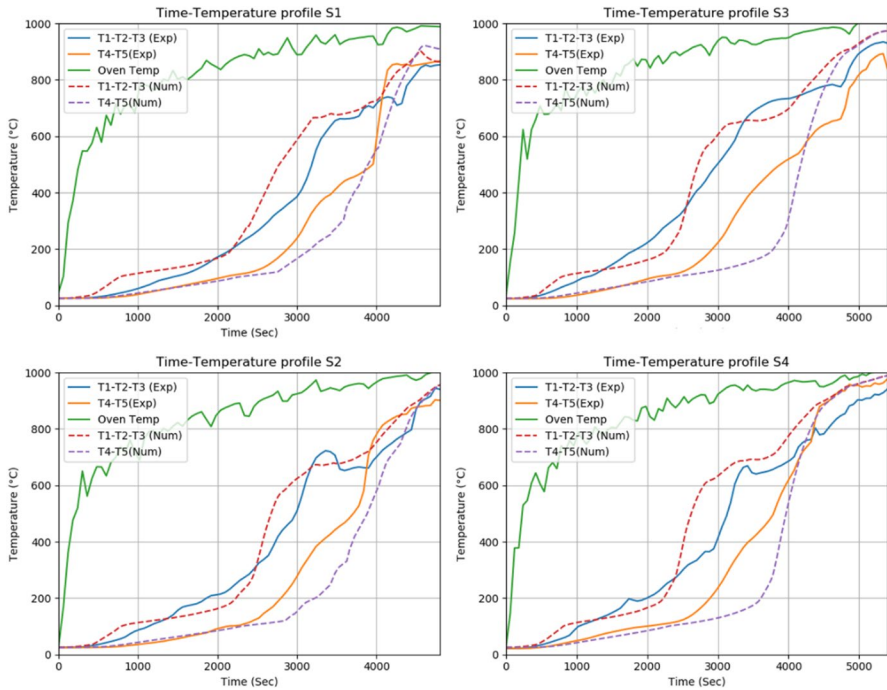


Fig. 16 Numerical temperature distribution for samples S1:4



**Fig. 17** Experimental and numerical Time–Temperature profiles for lower panels

the experimental and numerical time–temperature profiles start to rapidly increase. This occurs due to the exposure of the thermocouples to the air inside the furnace and the measurement of the temperature of the air, after the lower LVL layer is completely burnt.

The numerical temperature profiles from the measurement of inside temperature of the panels (T11–T12–T13) correspond well with the experimental temperature profiles, as shown in Fig. 18. The surface temperature slightly deviates from the experiments, likely due to charring of the upper LVL layer and slight movement of the thermocouples in this region. Oscillations are observed in the temperature profiles measured by the surface thermocouples of specimen S3, occurring between temperatures of 200°C and 350°C. These oscillations coincide with the ignition of the upper LVL surface and the formation of a charring layer, causing the thermocouples to shift from their initial positions. Once the surface is fully ignited, the thermocouples continue to record the rising temperature smoothly.

### Steel sheet profile

The homogeneous properties of the steel significantly contribute to the accuracy of the validation, as depicted in Fig. 19. The two stages of loading (radiation and convection), are clearly distinguishable from the elevated numerical temperatures observed in all the samples. Temperature profiles show a rapid increase after 50

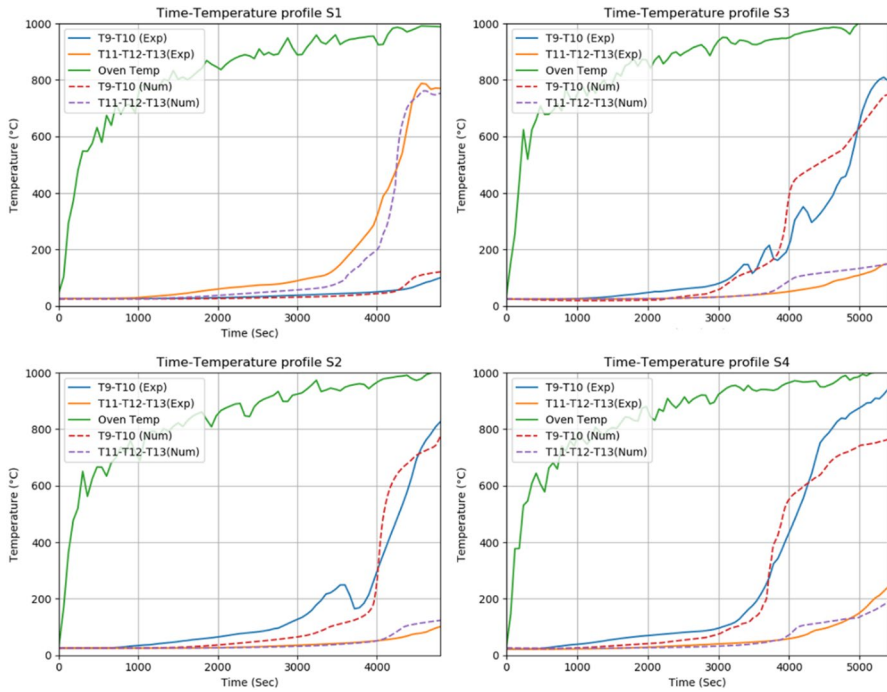


**Fig. 18** Experimental and numerical Time–Temperature profiles for upper panels

55 min, when the steel sheet is directly exposed to the furnace burner following the combustion of the lower LVL panel.

### Charring behavior

**Lower and upper LVL panels** To compute the charring rate of the lower panel, which is completely burnt during the test, the charring front temperature is set to 300°C (EN1995-1-2 2004). The charring duration begins when the thermocouples on the fire-exposed surface of the layer record 300°C, and it ends when the thermocouples at the inner surface of the layer record the same temperature. As shown in Fig. 20, the experimental charring rate of the panels averages between 0.7 and 0.73 mm/min, closely aligning with the recommended charring rate of 0.70 mm/min according to (EN1995-1-2 2004). Meanwhile, the averaged numerical charring rate is 0.74 mm/min. The numerical charring depths of the upper LVL panels show a uniform distribution across different cross-sections of the panel. Table 4 compares the experimental and numerical charring rates of upper LVL panels at three positions in the centerline, 150 mm above the centerline, and 150 mm below the centerline. Figure 20 compares the average experimental charring rates with the numerical results for different specimens of the WSH system. The upper LVL layers of specimens S1 and S2 ignite–surface thermocouples record 300°C—earlier than those of specimens S3 and S4. This discrepancy is attributed to the internal cavity influence, where the



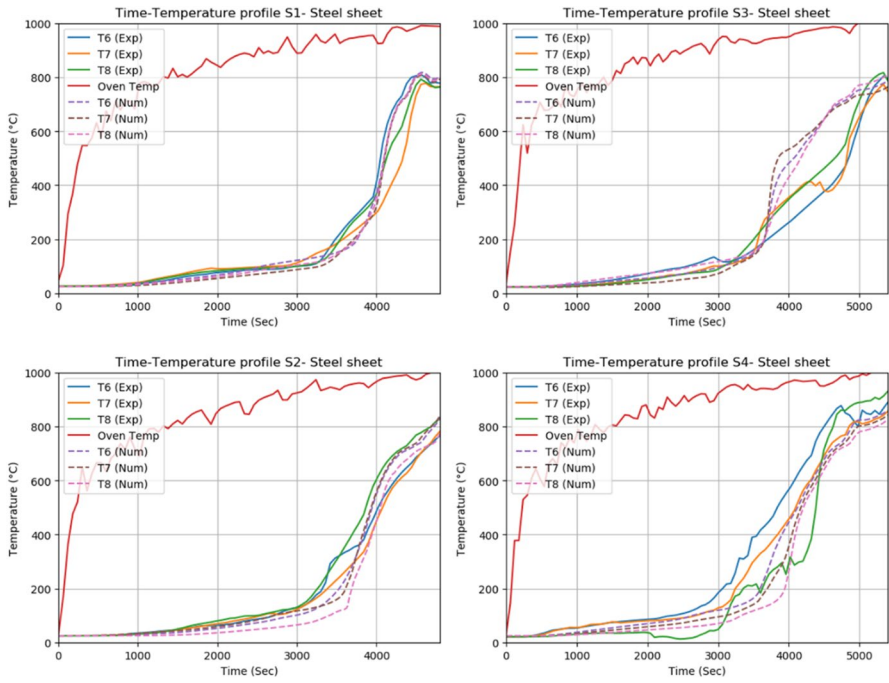


Fig. 19 Experimental and numerical Time–Temperature profiles for steel sheet profile

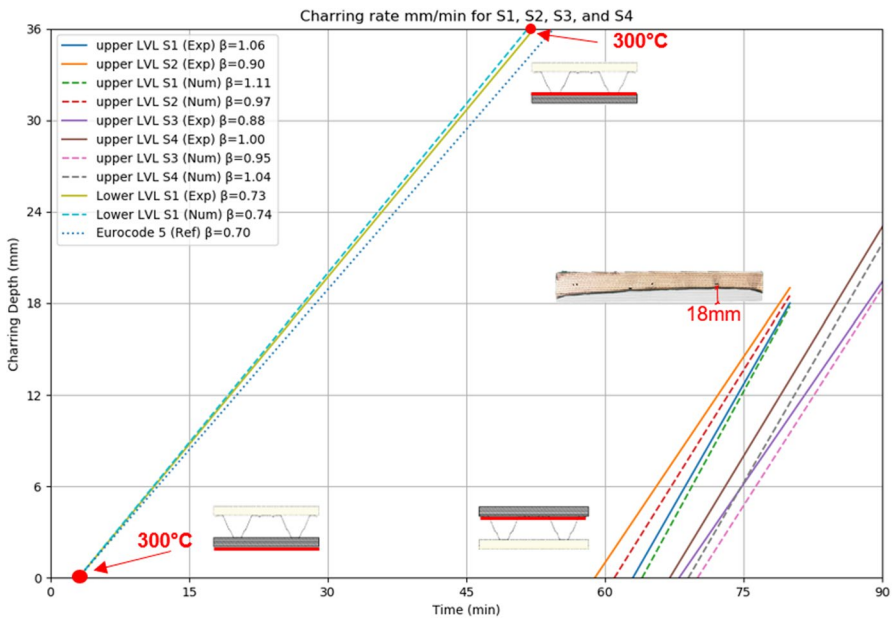
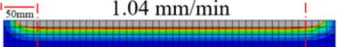
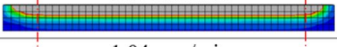
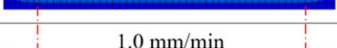
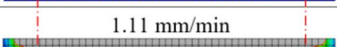
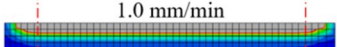
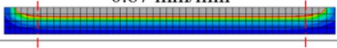
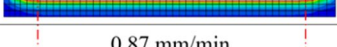
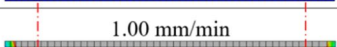
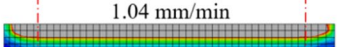
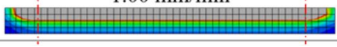
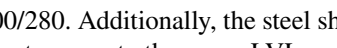
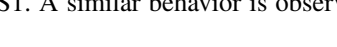


Fig. 20 Numerical and experimental charring rate mm/min for lower LVL panel

**Table 4** Experimental and numerical average charring rate of upper LVL panels

Specimen	Experimental charring rate	Numerical charring rate
S1	Sec a C.L.+150mm 1.00 mm/min	 1.04 mm/min
	Sec b C.L.(0.00) 1.06 mm/min	 0.97 mm/min
	Sec c C.L.-150mm 0.95 mm/min	 1.04 mm/min
S2	Sec a C.L.+150mm 0.92 mm/min	 1.0 mm/min
	Sec b C.L.(0.00) 0.95 mm/min	 1.11 mm/min
	Sec c C.L.-150mm 0.9 mm/min	 1.0 mm/min
S3	Sec a C.L.+150mm 0.76 mm/min	 0.87 mm/min
	Sec b C.L.(0.00) 0.88 mm/min	 0.95 mm/min
	Sec c C.L.-150mm 0.81 mm/min	 0.87 mm/min
S4	Sec a C.L.+150mm 0.96 mm/min	 1.00 mm/min
	Sec b C.L.(0.00) 1.00 mm/min	 1.04 mm/min
	Sec c C.L.-150mm 0.98 mm/min	 1.00 mm/min

steel section profile M150/280 is higher than M100/280. Additionally, the steel sheet thickness plays a notable role in transferring the heat energy to the upper LVL panel. The upper LVL of S2 ignites 4 min earlier than S1. A similar behavior is observed for S3 and S4.

The experimental charring rate for the upper panel averages between 0.88 mm/min and 1.00 mm/min, while the numerical charring rate averages between 0.95 mm/min and 1.06 mm/min, resulting in an average deviation of 5% to 8%. The increase in numerical results may be attributed to the conduction behavior between the panel and the steel profile, which is defined as tie contact in the model, allowing direct heat transfer to the upper layer without considering the gaps or imperfection in the contact surface. Another contributing factor could be the generic thermal properties of wood defined according to Eurocode (EN1995-1-2 2004), which may not accurately represent the behavior of the LVL element. The discrepancy observed aligns with findings from Couto et al. (2016), where deviations between numerical and experimental results in charring rate and temperature profiles were attributed to the effects of moisture content, which were not adequately considered in the numerical model.

To enhance numerical simulation results, researchers such as Špilák et al. (2022) and Molina et al. (2012) emphasize the importance of refining input material properties such as the thermal conductivity, specific heat capacity, and density of wood with temperature dependency in software models beyond the generic wood properties of softwoods and hardwoods specified in Eurocode-5 (EN1995-1-2 2004). However, one limitation of the current model is the use of generic LVL material properties derived from Eurocode 5, which may not fully capture the actual material behavior in more complex scenarios, such as when mechanical loading is applied during a fire. Additionally, the simplified thermal contact representation between the steel sheet and the LVL panels may not account for the effects of screws, air gaps, or other connection details under such complex loading conditions.

## Conclusion

In wood-steel hybrid slab systems, the geometrical configurations and thicknesses of both steel plate and LVL panels may play as a limiting role in the performance of the system under fire exposure. This study provided a numerical model to simulate the fire behavior of the components and predict the thermal performance of the hybrid system under fire. Additionally, fire experiments were conducted to validate the numerical models. The observations of this study can be summarized as follows:

- The size and shape of the internal cavity of the composite systems have a significant impact on the general fire resistance of the system. Furthermore, the configuration of the steel plate (especially height and thickness) strongly influences the fire performance of the upper LVL layer.
- Applying CT scanning after fire tests enhances our ability to assess density loss throughout the element thickness, which is a crucial indicator of material performance under fire conditions.
- The temperature profiles of the element components were well predicted numerically and validated against experimental data.
- The numerical prediction of the charring rate showed deviations of 5–8% from the experimental charring rate. This discrepancy is attributed to the crack formation during the fire tests and the generic thermal properties of wood as defined by Eurocode, which could be improved by refining the material model and redefining the thermal properties of LVL.
- The internal cavity of the element affected heat transfer; the upper LVL layers of specimens S1 and S2 with a steel profile height of 100 mm ignited earlier than those of specimens S3 and S4 with a steel profile height of 150 mm.
- The thickness of the steel profile notably influenced the charring rate; upper LVL layers connected to thicker steel profiles exhibited higher charring rates compared to those connected to thinner steel profiles.

Future work could include simulations using coupled temperature-displacement analysis to improve the prediction of thermo-mechanical performance in real-world scenarios. Additionally, exploring more detailed material models, considering the

effects of mechanical loading and temperature-dependent properties of LVL, along with further experimental validation, would enhance the accuracy and robustness of the numerical predictions.

**Acknowledgements** The authors gratefully acknowledge the support of the fire department group of Holzforschung München and the help of Dr. David Schinz and J. Kirschke from the Department of Neuroradiology at Klinikum Rechts der Isar for their contributions to this study.

**Author contributions** M.A.: Conceptualization, Investigation, Data curation, Methodology, Visualization, Writing—original draft A.K.: Conceptualization, Data curation, Methodology, Writing—review and editing. J.W.K.: Conceptualization, Review Editing, Supervision.

**Funding** Open Access funding enabled and organized by Projekt DEAL.

**Data Availability** No datasets were generated or analysed during the current study.

## Declarations

**Competing interests** The authors declare no competing interests.

**Open Access** This article is licensed under a Creative Commons Attribution 4.0 International License, which permits use, sharing, adaptation, distribution and reproduction in any medium or format, as long as you give appropriate credit to the original author(s) and the source, provide a link to the Creative Commons licence, and indicate if changes were made. The images or other third party material in this article are included in the article's Creative Commons licence, unless indicated otherwise in a credit line to the material. If material is not included in the article's Creative Commons licence and your intended use is not permitted by statutory regulation or exceeds the permitted use, you will need to obtain permission directly from the copyright holder. To view a copy of this licence, visit <http://creativecommons.org/licenses/by/4.0/>.

## References

- Abreu JCB, Vieira LMC, Abu-Hamd MH, Schafer BW (2014) Review: development of performance-based fire design for cold-formed steel. *Fire Sci Rev* 3(1):1. <https://doi.org/10.1186/s40038-014-0001-3>
- Balasanbeh AT, Sher W, Yeoh D (2022) Recommending a new building structure to alleviate environmental impact in tropical climates: Increasing the use of wood in construction. *Int J Life Cycle Assess* 27:885–901
- Couto DLP, Fonseca EMM, Piloto PAG, Meireles JM, Barreira LMS, Ferreira DRSM (2016) Perforated cellular wooden slabs under fire: Numerical and experimental approaches. *J Build Eng* 8:218–224
- Crielaard R, van de Kuilen J-W, Terwel K, Ravenshorst G, Steenbakkens P (2019) Self-extinguishment of cross-laminated timber. *Fire Saf J* 105:244–260
- Ehrlenspiel R, van de Kuilen J-WG (2012) Charring rate of laminated veneer lumber “BauBuche.” Technical Report, Technical University Munich, Munich
- EN 1363-1 (2012) European Committee for Standardization: Fire resistance tests - Part 1: General requirements. Brussels
- European Committee for Standardization. (2005) Eurocode 3: Design of steel structures—Part 1–2: General rules—Structural fire design (EN 1993-1-2:2005)
- European Committee for Standardization (2004) Eurocode 5: Design of timber structures—Part 1–2: General rules—Structural fire design (EN 1995-1-2:2004)
- Fahrni R, Schmid J, Klippel M, Frangi A (2018a) Correct temperature measurements in fire-exposed wood. In: Proceedings of World Conference of Timber Engineering WCTE 2018 Seoul, South Korea, <https://doi.org/10.3929/ETHZ-B-000289850>

- Fahrni R, Schmid J, Klippel M, Frangi A (2018b) Investigation of different temperature measurement designs and installations in timber members as low conductive material. In: Proceedings of the 10th International Conference on Structures in Fire FireSERT, Ulster University, Belfast, UK, June 6–8, 2018, <https://doi.org/10.3929/ETHZ-B-000269112>
- Fahrni R, Frangi A (2021) Model scale standard fire experiments on solid timber panels—charring and mass loss investigation to determine the variability of the charring rate, Report 2021–02. ETH Zurich. <https://doi.org/10.3929/ETHZ-B-000473150>
- Fonseca EMM (2024) Brief overview of the thermal and mechanical properties of wood, steel, and gypsum board for structural connections. *GeoStruct Innov* 2(2):77–89
- Fonseca EMM, Coelho DCS, Barreira LMS (2012) Structural safety in wooden beams under thermal and mechanical loading conditions. *Int J Saf Secur Eng* 2(3):242–255. <https://doi.org/10.2495/SAFE-V2-N3-242-255>
- Fonseca EMM (2013) Numerical model assess the fire behaviour of cellular wood slabs with drillings. In: Proceedings of the 4th International Conference on Integrity, Reliability, and Failure, Funchal, Portugal, ISSN 9789728826277
- Fragiacomo M, Menis A, Clemente I, Bochicchio G, Ceccotti A (2013) Fire resistance of cross-laminated timber panels loaded out of plane. *J Struct Eng* 139:04013018
- Frangi A, Fontana M (2003) Charring rates and temperature profiles of wood sections. *Fire Mater* 27:91–102. <https://doi.org/10.1002/fam.819>
- Frangi A, Erchinger C, Fontana M (2008) Charring model for timber frame floor assemblies with void cavities. *Fire Saf J* 43:551–564
- Freyburger C, Longuetaud F, Mothe F, Constant T, Leban J-M (2009) Measuring wood density by means of X-ray computer tomography. *Ann Sci* 66(8):804–804. <https://doi.org/10.1051/forest/2009071>
- Harada T, Uesugi S, Masuda H (2006) Fire resistance of thick wood-based boards. *J Wood Sci* 52:544–551
- Hassanieh A, Valipour HR, Bradford MA (2016) Experimental and numerical study of steel-timber composite (STC) beams. *J Constr Steel Res* 122:367–378. <https://doi.org/10.1016/j.jcsr.2016.04.005>
- Hsu T-L, Chang F-C, Tsai M-T, Le T-D-H (2016). Study on performance of timber-steel composite beams with different shapes of steel components. In: Proceedings of the World Conference of Timber Engineering WCTE 2016, Vienna, Austria
- Ilgin HE, Karjalainen M (2022) Perceptions, attitudes, and interests of architects in the use of engineered wood products for construction: a review. *IntechOpen*. <https://doi.org/10.5772/intechopen.92960>
- Incropera FP, DeWitt DP, Bergman TL, Lavine AS (eds) (2013) Principles of heat and mass transfer, 7th edn. Wiley, London
- Just A, Tera T (2010) Variability of charring along the wooden wall studs. *Const Struct Technol (Statyba Konstrukcijos Ir Technologijos)* 2:119–128
- König J (2005) Structural fire design according to Eurocode 5—design rules and their background. *Fire Mater* 29(3):147–163. <https://doi.org/10.1002/fam.873>
- Le TDH, Tsai MT (2019a) Behavior of timber-steel composite with dowel connection under fire. *Key Eng Mater* 803:195–199. <https://doi.org/10.4028/www.scientific.net/kem.803.195>
- Le TDH, Tsai M-T (2019b) Experimental assessment of the fire resistance mechanisms of timber-steel composites. *Materials* 12(23):4003. <https://doi.org/10.3390/ma12234003>
- Lindgren O (1992) Medical CT-scanners for non-destructive wood density and moisture content measurements (Doctoral dissertation, Luleå University of Technology, Department of Engineering Sciences and Mathematics, Wood Science and Engineering, Luleå), Doctoral thesis / Lulea University of Technology. ISSN 0348–8373:111
- Molina JC, Calil C, Kimura ÉFA, Pinto EM, Regobello R, Scheer MB, Carneiro C, Bressan OA, Santos KGD (2012) Numerical analysis of the behavior of timber elements under fire conditions. *Floresta e Ambiente (Forest and Environment)* 19(2):162–170. <https://doi.org/10.4322/floram.2012.019>
- Moss PJ, Buchanan AH, Fragiaco M, Lau PH, Chuo T (2009) Fire performance of bolted connections in laminated veneer lumber. *Fire Mater* 33:223–243
- Münker (2020) Trapezoidal cold-formed steel profiles. Retrieved from <https://www.muenker.com>. Accessed on 11 Dec 2024
- Nguyen MH, Ouldboukhite S-E, Durif S, Saulnier V, Bouchair A (2023) Passive fire protection of steel profiles using wood. *Eng Struct* 275:115274. <https://doi.org/10.1016/j.engstruct.2022.115274>
- O’Neill JW, Buchanan AH, Abu AK, Carradine DM (2013) The fire performance of timber floors in multi-storey buildings. Technical Report, Department of Civil and Natural Resources Engineering, University of Canterbury, Christchurch, New Zealand

- Petrycki AR, Salem O (2023) Structural fire performance of wood-steel-wood bolted connections with and without perpendicular-to-wood grain reinforcement. *J Struct Fire Eng* 14(4):441–460. <https://doi.org/10.1108/JSFE-02-2019-0016>
- Pollmeier (2017) BauBuche LVL. Retrieved from <https://www.pollmeier.com>. Accessed on 11 Dec 2024
- Rothoblaas (2010) Self-drilling timber-metal screws (SBS). Retrieved from <https://www.rothoblaas.com>. Accessed on 11 Dec 2024
- Špilák D, Majlingová A, Kačíková D, Tischler P (2022) Determining the charred layer of wooden beams with finite element analysis based on enthalpy approach. *Buildings* 12(7):875. <https://doi.org/10.3390/buildings12070875>
- Tabaddor M, Gandhi PD (2008) Thermal and mechanical finite element modelling of wood-floor assemblies subjected to furnace exposure, Underwriters Laboratories. Technical Report No. 07CA42520, File NC9140
- Thi VD, Khelifa M, El Ganaoui M, Rogaume Y (2016) Finite element modelling of the pyrolysis of wet wood subjected to fire. *Fire Saf J* 81:85–96. <https://doi.org/10.1016/j.firesaf.2016.02.001>
- Tsai M, Koshihara M (2014) The study and proposed application of the multi-storey hybrid timber structural system on design flexibility and hazard prevention. In: Proceedings of the World Conference of Timber Engineering WCTE 2014, Quebec, Canada
- White R, Dietsberger M (2010) Wood Handbook : Wood as Engineered Material, Chapter 18, Fire safety of wood construction. Department of Agriculture and Forest Service, Forest Products Laboratory, USA
- Yadav R, Kumar J (2022) Engineered wood products as a sustainable construction material: a review. In: Gong M (ed) Engineered wood products for construction. IntechOpen, London
- Yanchun L, Zhang Y, Bao W, Wang W, Liu Y (2021) Temperature variation of steel plates with different thicknesses on the normalizing process. *J Phys: Conf Ser* 1820:012127
- Zhang J, Xu Q-F, Xu Y-X, Wang B, Shang J-X (2012) A numerical study on fire endurance of wood beams exposed to three-side. *J Zhejiang Univ* 13:491–505. <https://doi.org/10.1631/jzus.A1200022>

**Publisher's Note** Springer Nature remains neutral with regard to jurisdictional claims in published maps and institutional affiliations.